Sensitivity Analysis of Geometric Imperfection Sources in Honeycomb Cores on Flatwise Compression Behavior

Adrian X. Rivera[1] and Satchi Venkataraman[2]
[1,2] San Diego State University, San Diego, CA, 92182, US

Hyonny Kim[3]
[3]University of California, San Diego, CA, 92037, US

Evan Pineda[4]
[4]NASA Glenn Research Center, Cleveland, OH, 44135, US

Andrew Bergan[5]
[5]NASA Langley Research Center, Hampton, VA, 23666, US

Manufacturing aluminum honeycomb core material using the expansion process can lead to geometric imperfections in the cellular core structures. These imperfections arise due to irregularities introduced in the initial foil bonding, variations in foil thickness, and residual stresses from manufacturing processes. Such geometric imperfections include cell shape distortions, cell wall waviness, non-uniform cell wall thickness, and variability in the shape and height of the adhesive fillet. Imperfections in the cell walls negatively affect the transverse compression and shear strength, while also reducing the resistance to damage under impact loads. Previous work presented the identification and quantification of these manufactured imperfections using high resolution X-ray computed tomography (CT) scans of honeycomb cores in co-cured composite sandwich panels. The present paper presents a sensitivity analysis of individual components of the sources of geometric imperfections on the flatwise compression of aluminum honeycomb cores. The initial geometric imperfections in honeycomb cells are decomposed into three components, namely cell shape (cell edge length and cell internal angles) in-plane cell wall waviness, and out-of-plane waviness along the core thickness. A sensitivity analysis is conducted using finite element (FE) models of the decomposed imperfections to understand how each component affects compression failure.

I. Introduction

Aluminum honeycomb core materials are lightweight cellular materials used in aerospace, automotive, marine structures, and sports protective gear because they provide a lightweight core material that can increase bending stiffness of sandwich panels and absorb impact energy. Aluminum honeycomb core is used in space structures to increase bending rigidity of structural panels by moving facesheets away from the neutral axis. The cellular structure of honeycomb cores provides a low-density material with high transverse normal and shear stiffnesses. However, honeycomb cores have poor ability to carry localized loads and are easily damaged under impact. Impacted honeycomb cores undergo crushing due to compressive and transverse shear stresses. The crushing response of honeycomb cores is initiated by buckling, followed by plastic collapse. To predict the impact and post-impact strength of honeycomb core sandwich structures, accurate and reliable models are required.

Honeycomb structures have been studied extensively for aerospace application as core material in sandwich construction due to the hexagonal lattice structure providing a low-density core material with beneficial transverse stiffness properties [1-4]. Optimal mechanical performance of honeycomb structures is predicated on maintaining a regular hexagonal shape [5]. Previous research has been shown through both experimental and numerical studies that deviation in the regular hexagonal shape results less optimal in-plane compression response as wells as in-plane

[1] PhD Student SDSU/UCSD Joint Doctoral Program in Structural Engineering, AIAA Member.
[2] Professor of Aerospace Engineering, AIAA Associate Fellow.
[3] Professor of Structural Engineering, AIAA Member.
[4] Research Engineer, Materials and Structures Branch, MS 49/7, AIAA Senior Member.
[5] Research Engineer, Durability, Damage Tolerance, and Reliability Branch, MS 188E, AIAA Senior Member.

compression failure [6,7]. McFarland [8] developed the theory of initial collapse of the cell structure and its subsequent progressive failure with analytical expressions for core crush strength and shear deformation. Wierzbicki [9] expanded this study by deriving analytical relations of the mean crushing strength of metal honeycombs as a function of the cell width, gauge thickness of the cell wall, and the yield stress of the material. Further work conducted by Wierzbicki and Abramowicz [10] showed that competing mechanisms at the single-double cell wall joint affect the kinematic crushing of the aluminum cell walls in transverse compression. Stretching at the joint due to bending along the yield surface influences the crushing morphology. During the initiation of crushing the yield surface can change orientation, minimizing plastic dissipation of aluminum cell wall post-elastic buckling. Wilbert et al [11] studied flatwise crushing of honeycomb cores and showed that cell wall imperfections (assumed first buckling mode shape) only moderately affect the crushing response. Janga and Kyriakides [12] investigated the effects of expansion of honeycomb material on the crushing response and showed that the onset of buckling was influenced by the degree of expansion. Cores that were expanded past the expected nominal geometry had reduced wall width with double thickness sections that resulted in a significant reduction in the critical stresses. Asprone et al [13] investigated the effect of cell wall imperfection in nomex honeycomb core using statistical distributions of varied material properties through the thickness of the core. The largest effect to compression strength was found to be variation in the wall thickness of the nomex core material. Relatively little published work exists on the effects of compression and shear response of honeycomb core with actual measured imperfections.

Typically, since imperfections in aluminum honeycomb are not precisely known, buckling mode shapes are used as seeded imperfections with an assumed amplitude to estimate the transverse normal strength. However, imperfections are dependent on design and the manufacturing process and therefore and may not resemble the first or higher buckling mode shapes. Since buckling is the primary driver of crushing, determining the exact nature and source of the initial geometric imperfections becomes important. The process of producing honeycomb cores starts with adhesively bonding sheets (foils) together, then cutting the sheets into strips for the desired core height, and finally expanding the bonded strips. The expansion direction (W-direction) is normal (to the sheet/ribbon direction (L-direction). Deformation of the foils during the expansion process forms plastic hinges at the ends of the bonded widths. In an ideal case these expanded cores will have regular hexagonal structures, with the double thickness wall along the bonded segments (L-direction). In the present cases, a co-cure cycle bonds facesheets to the core material, while also curing the pre-pregnated laminas, which introduces thermal residual stresses due to the mismatch in coefficients of thermal expansion resulting in geometric imperfections. In the previous work by Campbell [14] it was described that an autoclave co-cure process requires pressure to suppress porosity in the laminas which can lead to facesheet dimpling as well as core crushing and core migration. Tavares et al. conducted a series of studies [15, 16] analyzing the influence of prepreg air permeability on the core pressure during processing. They showed that the gas pressure within the core can influence fillet geometry, skin-to-core distance, and adhesion strength; furthermore, claimed an optimal range of core pressures exists that could optimize adhesive strength. They investigated the behavior of fully impregnated prepreg and partially impregnated (with a much higher out-of-plane permeability), which enabled enhanced core evacuation but was also prone to exhibiting resin bleed into the core. These sources of manufactured induced geometric imperfections result in unique manufacturing signature in aluminum honeycomb core and their effect on the mechanical response have not been thoroughly explored in the present literature.

The present state of the art lacks models that accurately capture measured manufacturing induced imperfections in honeycomb core and the understanding of the effects of imperfections on compression strength. This paper discusses a novel approach of using X-ray CT to reconstruct finite element shell models of honeycomb cores with measured manufacturing imperfections. In Section II details of the X-ray CT are discussed and presents measured imperfections from specimens of the same sandwich material system but manufactured in different batches. Section III describes the finite element models with as-manufactured imperfection that are decomposed into models with specific imperfections removed to understand the sensitivity specific sets of imperfection have on compression strength. The results are discussed in section IV of the paper in which model validation is shown via flatwise compression experiments of the imaged specimens. A comparison of the different imperfection cases are shown through stress-strain compression plot and through-thickness compression stiffness behaviour.

II. Characterization of Aluminum Honeycomb Core Geometric Imperfections

The availability of X-ray computed tomography (CT) imaging and image processing techniques [17] has led to the precise characterization of imperfections and crushed cores of sandwich honeycomb cores. The honeyomb core

sandwich samples of a size 2 in. by 2 in. and thickness of 1.0 inch were imaged using X-ray CT. The scans were perfomed using a X-RAY WorX 80 watt source and a Dexela 2923 detector configured such that the source was 200 mm from the specimen and 760 mm from the detector. The scans captured 1800 projections resulting in 1410 image slices through the thickness of the specimen (1.085") and a typical voxel size of 20 μm [18].

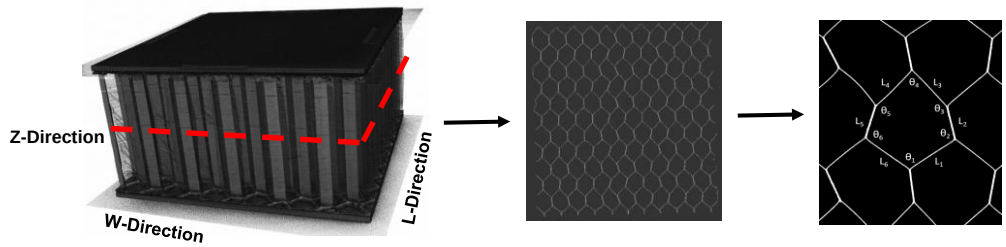

Fig. 1 X-ray CT image of aluminum honeycomb core sandwich composite (a) 3D volume reconstruction of a 2 in. by 2 in. specimen showing the honeycomb core material axes, (b) mid-plane cross section of the volume, and (c) magnified view of a single cell and labels corresponding to the internal angles and cell walls.

Table 1. Measured values of honeycomb internal angle and cell wall lengths from Figure 1c.

Label	*Angle θ (°)*	*Length L (in)*
1	*106.1*	*0.115*
2	*115.6*	*0.077*
3	*152.5*	*0.112*
4	*84.2*	*0.110*
5	*151.3*	*0.077*
6	*110.3*	*0.117*

Figure 1(a-c) shows the reconstructed volume and cross-section view at the mid-plane of a 2 in. by 2 in. honeycomb core specimen obtained using the X-ray CT. These images show the in-plane cell shapes deviate from the perfect/ideal hexagonal geometry. The cells exhibit variations in edge length and cell internal angles as well as waviness of the walls. Table 1 presents measurements of the internal angles and lengths of the cell walls of the hexagonal lattice in figure 1c, showing the resultant in-plane cell geometry after the manufacturing process. Image analysis of the honeycomb cells showed the as-manufactured sandwich core has cell shape variations which deviate from an ideal honeycomb geometry. Figure 2 presents the 3D reconstruction of the isolated single cell (figure 2a), the mid-plane (W-L) geometry of that cell (figure 2b), and the through thickness (W-Z) cell walls (figure 2c). The single cell walls highlighted in red and double cell walls highlighted in blue have a unique through thickness waviness induced by the manufacturing (in an ideal core the cell wall would not translate nor have variation in the L-Z plane or W-Z plane).

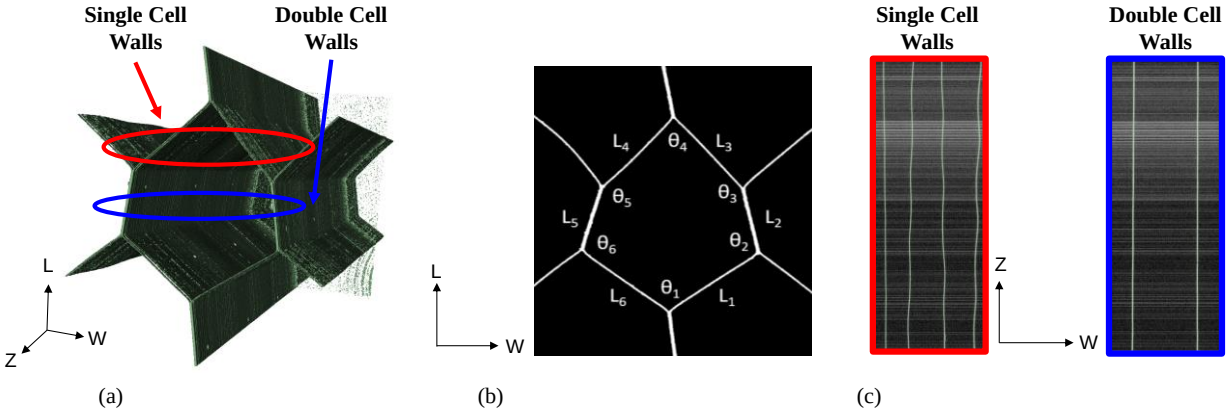

Fig. 2 X-ray CT of a honeycomb core (a) 3D image reconstruction of single cell (W-L-Z) (b) cross section image at the mid-plane (W-L) (c) W-Z plane showing a series of single cell walls and double cell walls transverse through the core.

The X-ray CT images reveal that the geometric imperfections in honeycomb cores can be classified as in-plane shape variation (cell edge length and cell internal angles), in-plane cell wall waviness, and out-of-plane waviness along the core thickness direction. The cell shape imperfections (without waviness in the cross-section plane or thickness direction) can be further decomposed into three subcomponents, namely cell size, cell aspect ratio, and cell internal angle change. Variation in cell size inherently affects the apparent density of the core material and the response under compression loading in the z-direction. Variation of the aspect ratio of the cells arises as a result of either over- or under-expanding the core. Depending on the degree of expansion the angles between the double thickness bonded cell walls and the single thickness cell walls, change accordingly to maintain an irregular hexagonal shape. Variation in cell wall lengths and added distortions to the cell geometry also leads to internal angle changes of the honeycomb cell; in addition, introduces a loss of reflective symmetry that induces anisotropy. For these reasons, the cell shape variations were parameterized and investigated individually. Samples from two different honeycomb core sandwich panels were imaged using X-ray CT and analyzed. Initial investigation showed that one set of panels had under-expanded (UE) cores and the other had over-expanded (OE) cores. This nomenclature refers to the geometric distribution of the internal cell size of each batch in which the cell size is less than or greater, respectively, than the nominal cell size reported by the manufacture (0.1875 inch). Table 2 shows the mean values of the in-plane angles of the core cells and the mean value of the cell size (here cell size is quantified by the length between the two bonded double wall of the honeycomb core) from the specimens that were imaged prior to testing under flatwise compression.

Figures 3-6 present the cell internal angle variation on the mid-plane and cell size variation though the thickness of the core for the two UE and two OE cores. In both batches we see similar angle distributions establishing a characteristic imprint that the expansion process has on honeycomb core manufacturing. Yet, in the OE core angles 1 and 4 are larger compared to UE cores as these are the angles orthogonal to the expansion direction. The measured average cell size of the 2 in. by 2 in. compared to the moving average as a function of the z-direction reveals morphing in-plane geometry of the internal cells as a result of the through thickness waviness of the cell walls. From these plots the honeycomb core is shown to exhibit significant spatial variation unique to each a 2 in. by 2 in. sample.

Table 2. Geometric measurements from X-ray CT of the internal cell angles and size of the aluminum honeycomb core specimens

Mean Values	θ_1	θ_2	θ_3	θ_4	θ_5	θ_6	*Cell Size (in)*
UE 1 As-manufactured	*89.4*	*121.5*	*145.4*	*104.26*	*119.1*	*151.3*	*0.1807*
UE 2 As-manufactured	*89.6*	*122.3*	*146.7*	*103.2*	*120.4*	*150.6*	*0.1801*
OE 1 As-manufactured	*96.9*	*116.4*	*145.3*	*108.5*	*116.8*	*142.7*	*0.1899*
OE 2 As-manufactured	*97.0*	*116.4*	*143.7*	*108.6*	*115.4*	*143.9*	*0.1900*

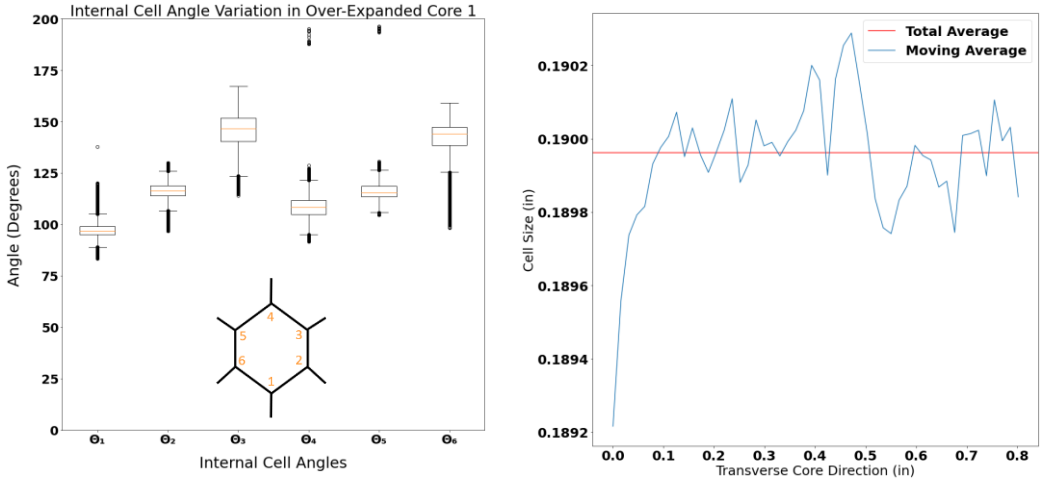

Fig. 3 Geometric measurements of internal angles and cell size through the core thickness for over-expanded core 1 sample.

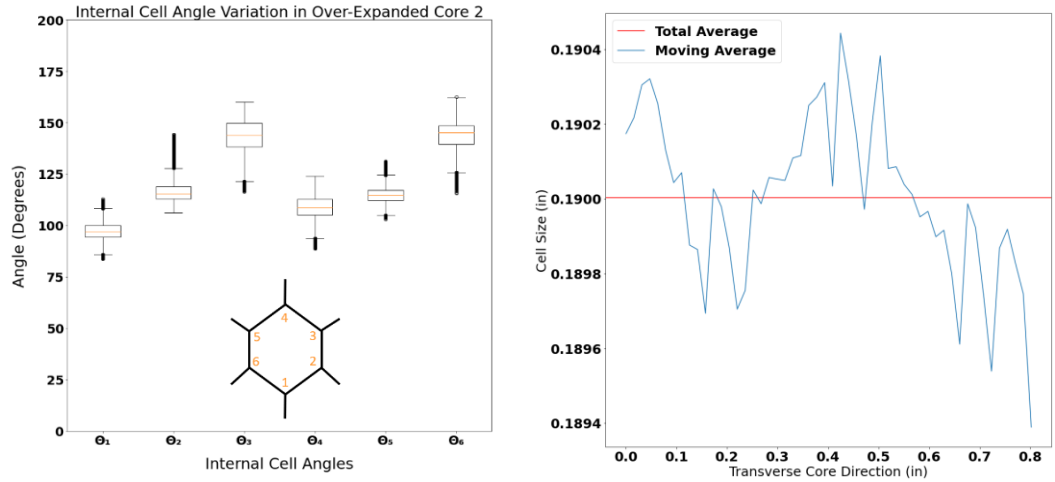

Fig. 4 Geometric measurements of internal angles and cell size through the core thickness for over-expanded core 2 sample.

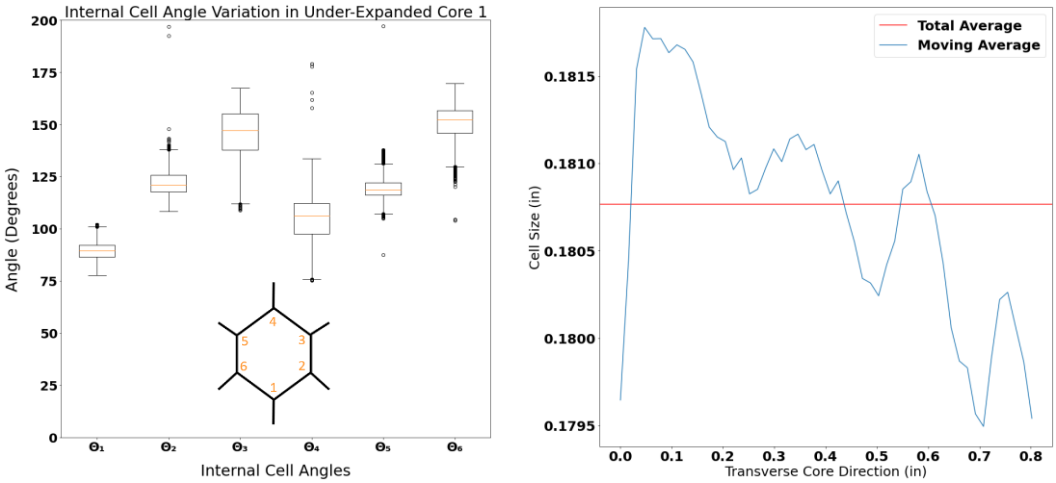

Fig. 5 Geometric measurements of internal angles and cell size through the core thickness for under-expanded core 1 sample.

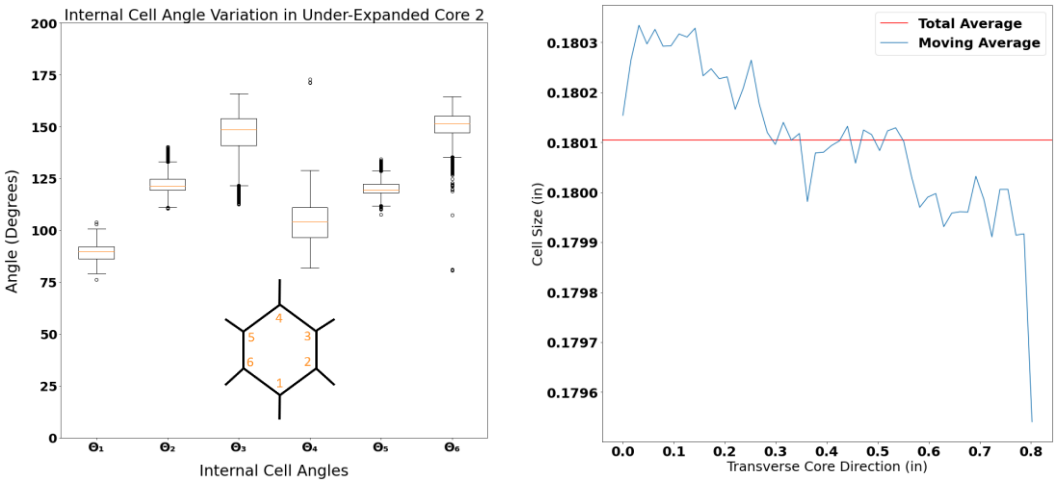

Fig. 6 Geometric measurements of internal angles and cell size through the core thickness for under-expanded core 2 sample.

In this paper we present a sensitivity analysis of the imperfection components on the nonlinear through thickness compression behavior. For this, the measured imperfection are decomposed into components. The geometric imperfection parameters considered in this study are cell size, internal angles, bonded cell face width, in plane cell wall curvatures, and cell wall waviness through thickness direction (Z-direction). The positions of the cell wall through the thickness were averaged, and the mean positions used as the cell wall geometry to eliminate cell wall waviness along the thickness direction. Next, nodal locations of the honeycomb cells were identified and connected by straight lines to eliminate in-plane cell wall waviness and obtain model having only honeycomb cell shape deviations (cell wall edge length and cell wall angles). Figure 7 shows a schematic representation of the different imperfection cases investigated.

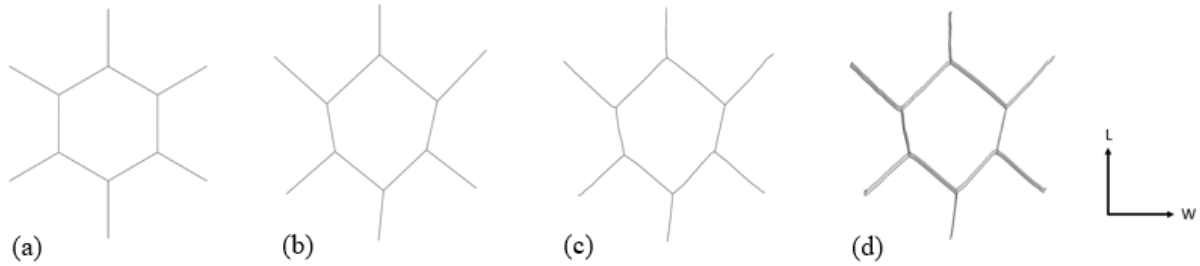

Fig. 7 Honeycomb cell geometries for the imperfection cases a) idealized geometry b) angle variation with straight cell walls c) angle variation with curved cell walls d) as-manufactured geometry containing in-plane and out-of-plane imperfections.

III. Details of Finite Element Model with Imperfections

In previous work, Rivera et al. [18], characterized honeycomb core imperfections using X-ray CT scanning and image processing, and computationally modeled the honeycomb cores with the X-Ray CT measured cell wall imperfections. A series of numerical finite element models were constructed from CT imaging data that captures the imperfections present in a 2 in. by 2 in. size core (approximately 121 individual cells). These 2 in. by 2 in. specimens were also physically tested under flatwise compression loads. Comparison of analysis model showed that the models with as manufactured imperfections lead to different crushing responses compared to the ideal honeycomb core model as well as from the honeycomb core modeled with imperfections seeded using buckling mode shapes.

The goal of paper is to quantify the influence of individual and interaction effects of these parameters on compression strength. Finite element analysis of the compression response was performed, with honeycomb core models discretized with linear shell (S4R) elements with a typical element size of 0.005 inches. The numerical method implemented was an explicit forward Euler using the Abaqus/Explicit finite element solver with a period of 1 second and a mass scaling increment value of 1e-6 to maintain a quasi-static analysis. The core height was limited to 0.8 inch as this represents the distance between the adhesive fillets in the CT imaged sandwich honeycomb samples (1.0-inch-thick cores is the specimen height). The honeycomb material was assumed to have elastic perfectly plastic material behavior which is substantiated by the experimental data reported by Lerch [19]. Figure 8 shows the boundary conditions for the full 10x11 cell model representative of the flatwise compression tests where the top and bottom nodes are constrained except at the applied displacement where the outer edges are free to displace and rotate.

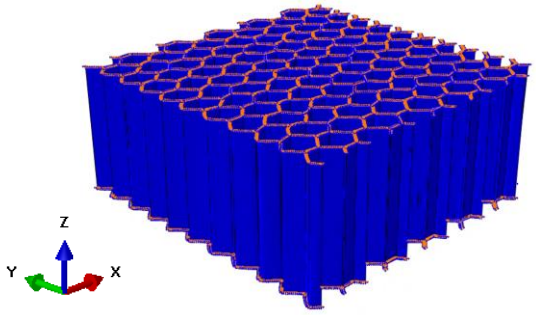

Fig. 8 Applied boundary conditions at top and bottom edges (fixed except at applied displacement) and free along the outer edges.

IV. Results

This section presents results of the validation of finite element analyses of honeycomb cores under transverse compression loading as well as the finite element analysis with the measured imperfections and the decomposed components as discussed in the previous section for the four samples imaged (and listed in Table 2). The nominal compression stress versus enforced compression displacements along the thickness direction are compared. Stress-displacement responses are also quantitatively compared by extracting the elastic compression modulus of the core, the peak stress during collapse, the stress at which plastic deformation initiates, the plastic modulus (tangent modulus of the core after initiation of plastic deformation), and the elastic buckling stress for each case. The nominal stresses are computed by dividing the total reaction forces by the cross-sectional area of the 10x11 cell models (square area of 2 in. by 2 in. sample that was X-ray CT imaged and tested). The first loading instant at which an 0.05% percent instantaneous drop in the transverse stiffness, prior to any plastic deformation, is reported as the elastic buckling stress. The results were checked to ensure that this was due to elastic buckling and there is no plastic strain is zero in the model. In cores with wall waviness imperfections the transverse loading leads to amplification of the initial imperfections. However, since imperfections are different in the single and double cell walls of the core. The cores exhibit a mode switching that leads to similar drop in transverse stiffness.

A. Validation of Finite Element Models Under Compression Loading

Flatwise compression tests were conducted following ASTM C365 standard [20] on sandwich specimens sectioned to a size of 2 by 2 inch from the UE and OE core sandwich batches. Two specimens, that were previously imaged using X ray CT, were tested from each batch. The test specimens were cut from sandwich panels with quasi-isotropic $[+45/90/-45/0]_s$ with facesheets of IM7/8552 material and a 1.0-inch-thick aluminum 5052 honeycomb core with a density of 3.1 pcf. (lb/ft^3). The test was conducted in displacement control at a loading rate of 0.025 in/min. (quasi-static conditions). The local strains were measured through virtual extensometer from a digital image correlation system (Aramis). The compression models were validated by the experimental (figure 9) capturing the compression response for each specimen with its unique manufacturing induced imperfections. The compression strength prediction for all cases were within 5 percent of the experimental results. The compression response in both experimental and finite element prediction behaved with an initial elastic regime followed by the non-linear elastic response from the amplification of initial imperfections. The failure is than characterized as an elastic-plastic buckling that initiate crushing of the honeycomb core. The post-peak response under predicts the softening behavior this as the models assume perfectly plastic yielding for the aluminum foil material. The post yield and crushing response of the honeycomb core can be better predicted if the hardening behavior of the aluminum foil material can be accurately characterized and implemented into the current model with as-manufactured imperfections. The assumption made in the models that the foil behaves perfectly plastic oversimplifies the reality that the foil material which does not have a poly-crystalline structure due to the repeated rolling worked into the material to achieve the thin wall features.

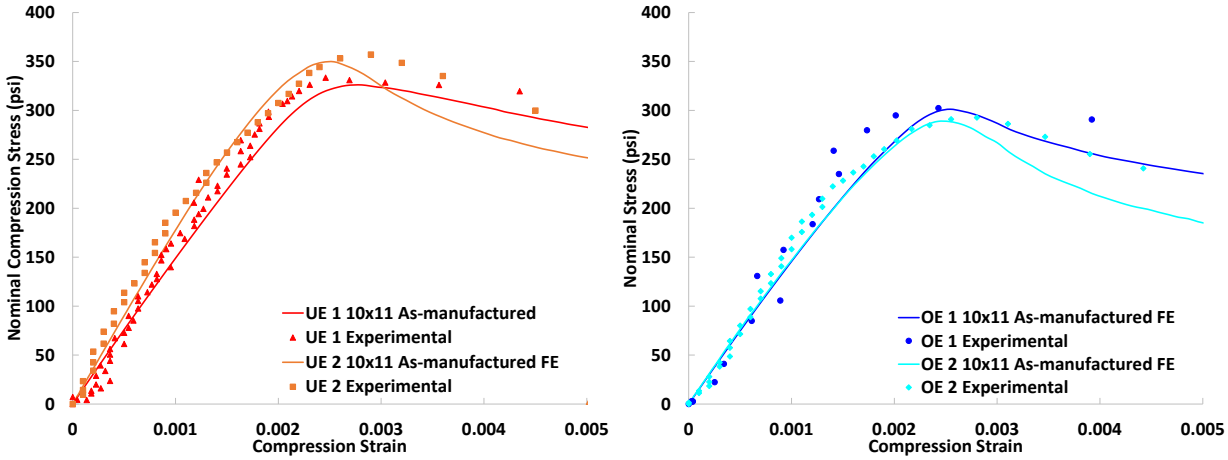

Fig. 9 Compression strain versus stress plots comparing the finite element models with as-manufactured imperfections to the respective flatwise experiment test.

B. Finite Element Analysis of Imperfection Cases

The 10x11 cell models have the shape imperfections generated from the experimental compression specimens X-ray CT. By comparing the decomposed imperfections compression response, elastic regime, and post-buckling regime the mechanics of how imperfections effect the compression response of aluminum honeycomb cores will be understood. Figures 10 and 11 shows the compression response (stress versus compression strain) of the honeycomb core from all imperfection cases. The post-peak response has an average drop in compression strength of 28.3 percent where it settles in the crushed state in the model with angle variation and in-plane curvature imperfections. The as-manufactured models show a post peak response in which the initial compression strength drops 17.3 percent. However, there is significant scatter among the cases analyzed in the post-yield crushing strength. Comparing the two batches of modeled specimens we see similar behavior for the angle variation and in-plane waviness imperfections in which at 0.1 percent strain there is change in the stiffness response which is maintained until the on-set and evolution of yielding.

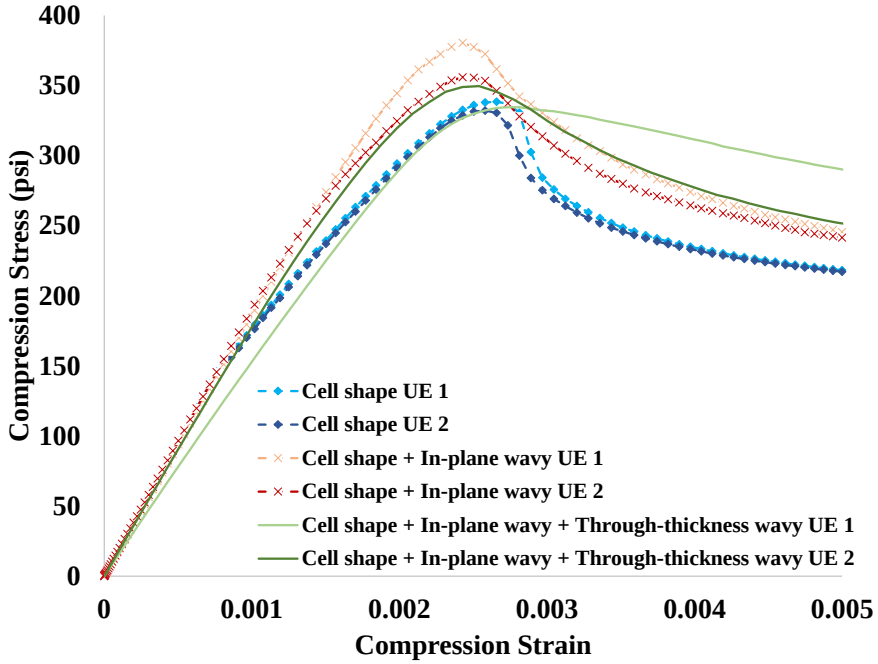

Fig. 10 Compression strain and stress plots with angle variation, in-plane curvature, and as-manufactured cases for UE 10x11 cell models.

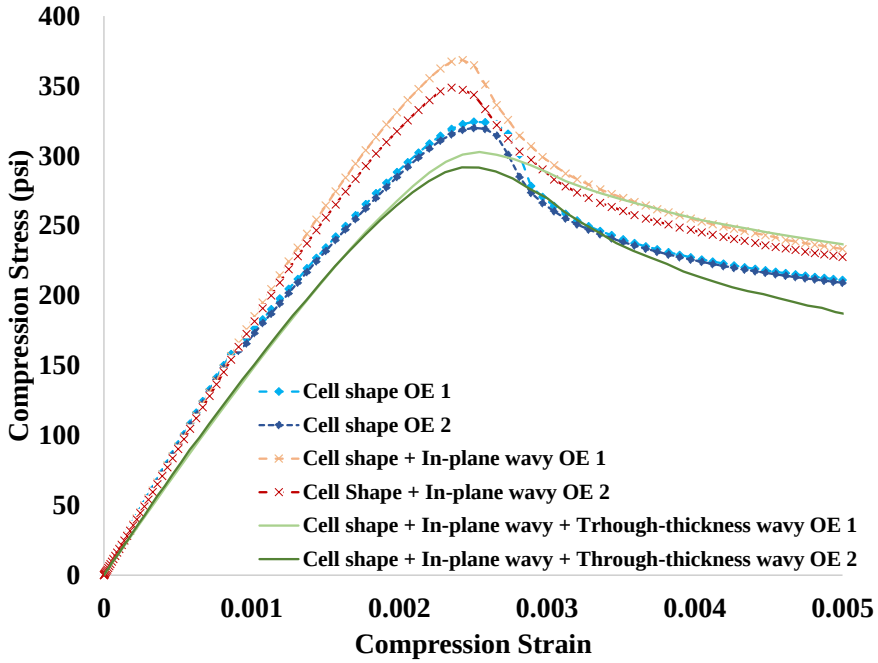

Fig. 11 Compression strain and stress plots with angle variation, in-plane curvature, and as-manufactured cases for OE 10x11 cell models.

The morphology of the crushing response is shown to significantly dependent on the imperfections this is shown in figure 12 and 13 in which the stress-strain response of the OE 1 specimen is segmented into regions of interest and the displacement magnitude contours are shown for the corresponding regions respectively. The honeycomb cores with only cell angle and cell edge length variations exhibit buckling earlier than the cores with in-plane waviness shown in figure 13(a-II) and 13(b-II). The non-linear geometric stiffening provided by the in-plane waviness imperfection delays onset of buckling and thereby reaches a higher peak compression stress (figure 13(b-III)). The formation of buckling shapes in the displacement contour of the model with in-plane waviness in figure 13(b-III) are concentrated in the single cell walls while the double cell walls stabilize the core until crushing failure. Furthermore, figure 13(c-I) to 13(c-III) shows the displacement contours of the compression response of the honeycomb cores having both in-plane and out-of-plane imperfections (here referred to "as-manufactured" models). The addition of wall waviness in the thickness direction (compression load direction) induces from the on-set of loading amplification of initial imperfections. At 0.2 percent strain the as-manufacture model (figure 13(c-III)) shows the largest amplification of imperfections to be within the single cell walls of the specimen. In all cases the plastic limit is reached in which the cell walls begin to fold from large out-of-plane due to the amplification of the initial buckling mode or the amplification of the dominant imperfection shape when cell wall waviness along thickness is considered.

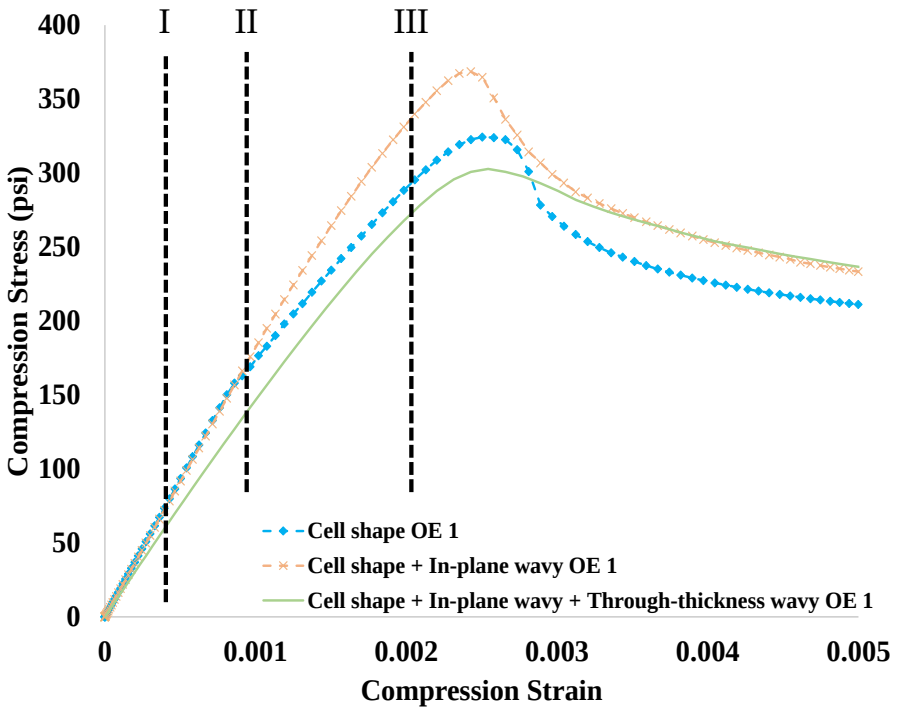

Fig. 12 Compression strain and stress plots of imperfection cases for OE 1 10x11 cell models with areas of interest marked at I) 0.05 percent strain, II) 0.1 percent strain and III) 0.2 percent strain.

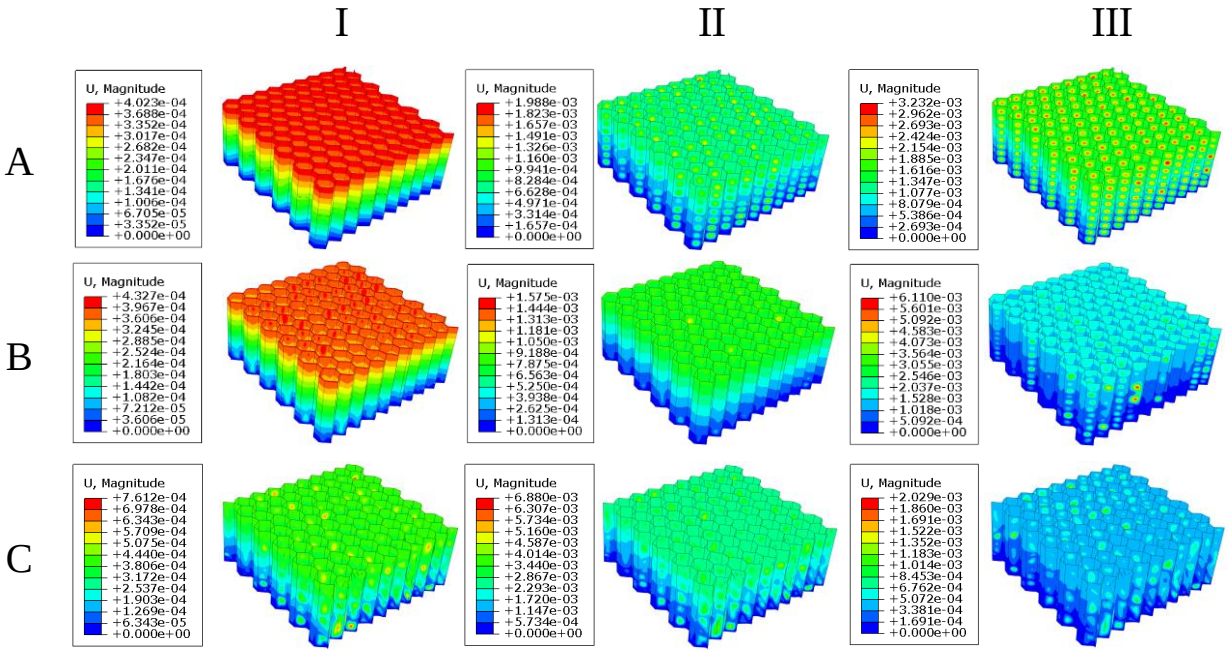

Fig. 13 Displacement magnitude contours of a) angle variation, b) in-plane curvature and c) as-manufactured for regions of interest I) 0.05, II) 0.1 and III) 0.2 percent strain.

Figure 14 and 15 plots the through-thickness secant stiffness, which is defined as the secant slope at every loading increment using the origin as the initial reference point, of the honeycomb cores computed from the stress versus

displacement data plotted in Figures 10 and 11. These plots show the sudden drop in stiffness for cores having only cell shape variations and no waviness in the cell walls, indicating that these cores experience elastic buckling first followed by amplification of the buckling induced deformation that leads to plastic collapse. In both batches of honeycomb cores, the case that includes only angle deviations results in a significant drop of through-thickness stiffness at around 50 percent of the compression strength. In this regime the failure is dominated by the on-set of elastic buckling followed by plastic strain accumulation due to the increase in local bending of the cell walls. It can also be seen addition of in-plane wall waviness leads to a small decrease initial stiffness but delays the onset of buckling due to the non-linear geometric stiffening introduced by the cell wall curvature. However, introduction of the wall waviness along the through thickness direction leads to significant drop in the stiffness and reduction in the peak stress reached. The early amplification of initial geometric imperfection under the compression load leads to earlier onset of plasticity and collapse.

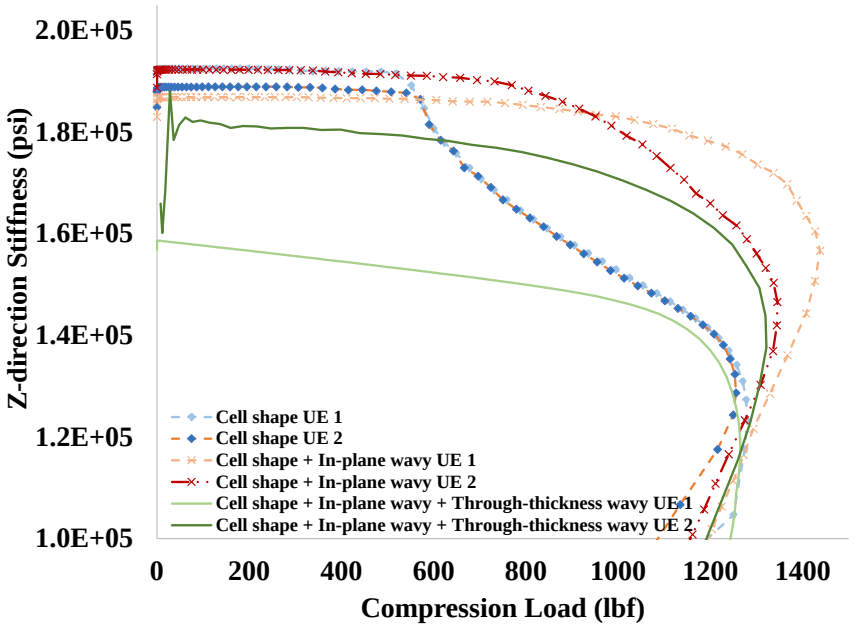

Fig. 14 Through-thickness stiffness and compression load plot of UE 10x11 models.

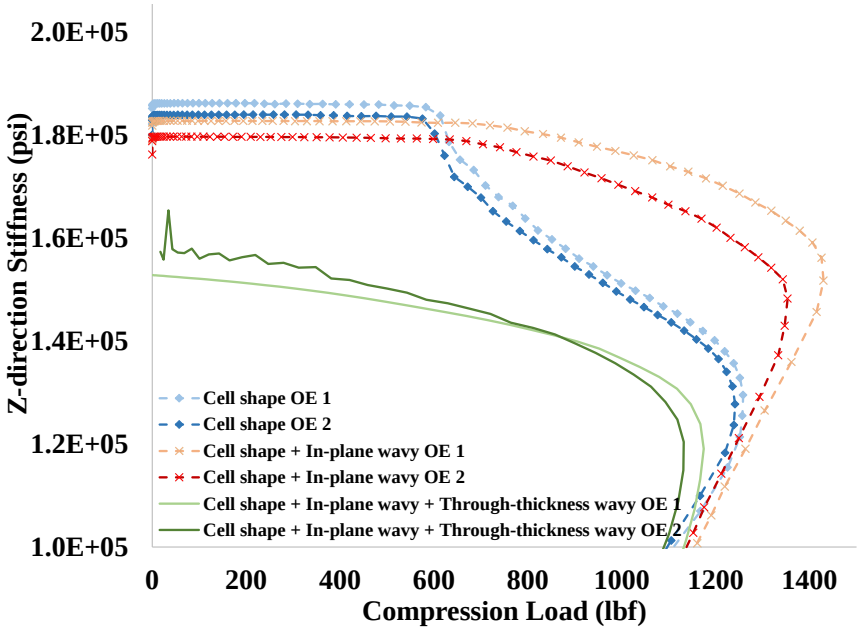

Fig. 15 Through-thickness stiffness and compression load plot of OE 10x11 models.

The non-linear compression response observed can be characterized by four metrics, namely, initial elastic stiffness, load for initial/elastic buckling, tangent plastic modulus and peak compression stress Table 3 shows a comparison of these four metrics for the OE and UE cores analyzed with different components of the measured geometric imperfections. The results are also graphically presented in Figures 16 and 17. Imperfection sensitivity results presented din Table 3, Figures 13 and 14 show that the compression modulus of cores modelled with all components included (as-manufactured) are 14.2% and 9.8% lower than the cores with only in-plane imperfections. There is no difference in stiffness between cores with only cell shape imperfection or those with both cell shape and in-plane waviness imperfections. The in-plane waviness help stabilize the core for buckling resulting in higher initial buckling load and final collapse load. This imperfection negates some of the effects of wall waviness imperfection along transverse core direction. The cores analyzed with cell wall waviness in the thickness direction exhibit very low buckling loads. The initial imperfections have multiple wavelengths present and are different in the single and double thickness wall of the cells. Interaction of the buckling shapes at the single cell and double cell wall joints leads to mode switching in which out-of-phase buckling shapes will force crushing in those locations.

Table 3. Comparison of different metrics of compression response of honeycomb cores with different imperfections components

	Compression Modulus E_z (ksi)	*Buckling Stress (psi)*	*Stress at Plastic Strain Initiation (psi)*	*Peak Nominal Stress (psi)*
Angle Variation				
UE 1	*192.4*	*137.1*	*179.2*	*338.4*
UE 2	*188.8*	*142.9*	*151.1*	*323.5*
OE 1	*186.1*	*150.2*	*162.2*	*324.4*
OE 2	*179.6*	*139.8*	*148.4*	*319.9*
In-Plane Curvature				
UE 1	*186.8*	*160.2*	*189.5*	*380.4*
UE 2	*193.3*	*154.8*	*193.6*	*355.8*
OE 1	*182.7*	*166.2*	*224.4*	*368.5*
OE 2	*179.6*	*154.1*	*209.3*	*348.8*
As-manufactured				
UE 1	*158.5*	*20.3*	*117.5*	*325.5*
UE 2	*182.8*	*25.0*	*167.1*	*349.6*
OE 1	*152.4*	*17.0*	*116.5*	*295.3*
OE 2	*157.0*	*17.5*	*118.2*	*291.7*

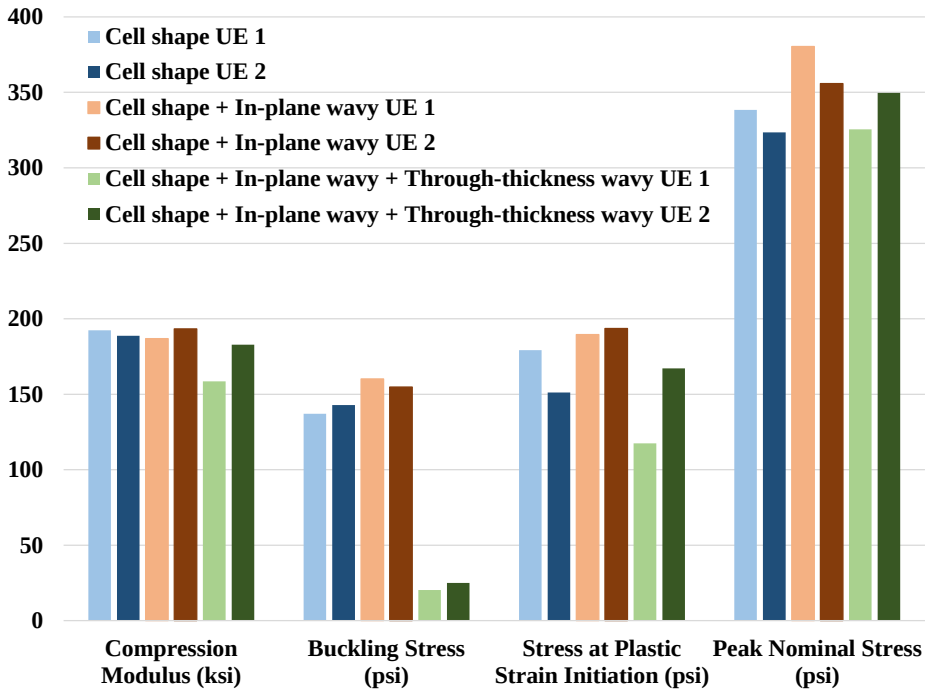

Figure 16: Comparison of imperfection sensitivity of under-expanded (UE) honeycomb core to different imperfection components.

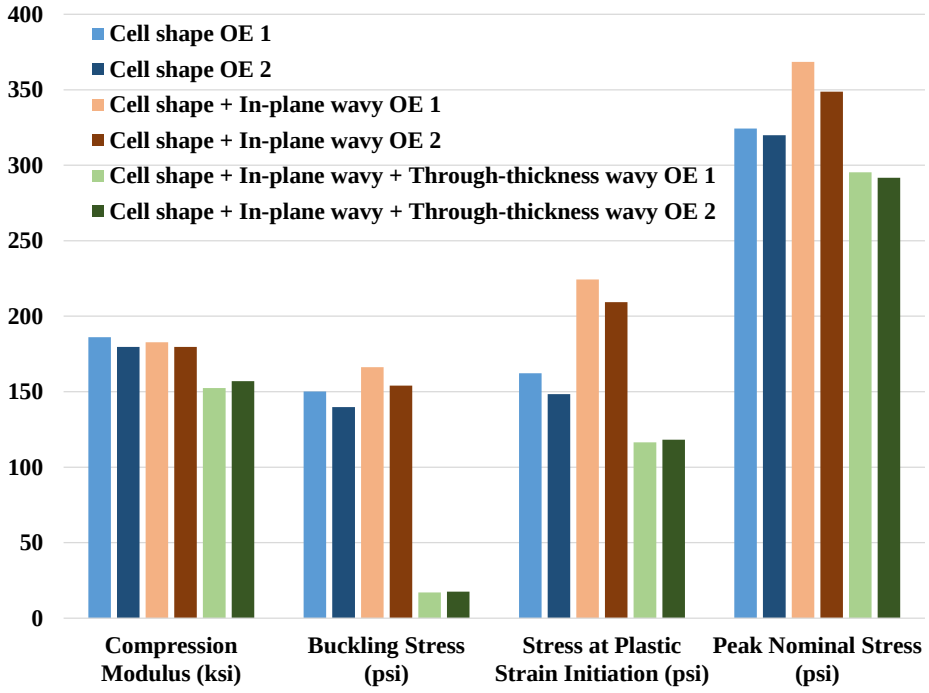

Figure 17: Comparison of imperfection sensitivity of over-expanded (OE) honeycomb core to different imperfection components.

Figure 15 shows the von-mises stresses at 95 percent of peak compression stress for each imperfection case. In the angle variation models, the stress field is distributed symmetrically on the honeycomb cell walls reaching the yield stress at every single and double cell wall (shown in the red contour mapping in figure 15). The yielding of the model with only cell shape imperfections mirrors the initial elastic buckling mode shape. The in-plane curvature model has a stress field in which yielding has occurred predominantly in the single cell walls, but the in-plane curvature allows for higher stresses along the double cell walls prior to the complete crushing failure of the honeycomb core (figure 18(1b, 2b, 3b and 4b)). The as-manufactured model has localized yielding at single cell walls and begin to propagate into the double cell walls (figure 18 (1c, 2c, 3c, and 3c)). The distribution of the foil yielding is dependent on the through-thickness initial shape in which locations of high out-of-plane waviness promotes the amplification of imperfections that initiates yielding. Imperfections through the thickness of the core contribute to a non-uniform stress field due to stress concentrates at locations in which imperfections are being amplified.

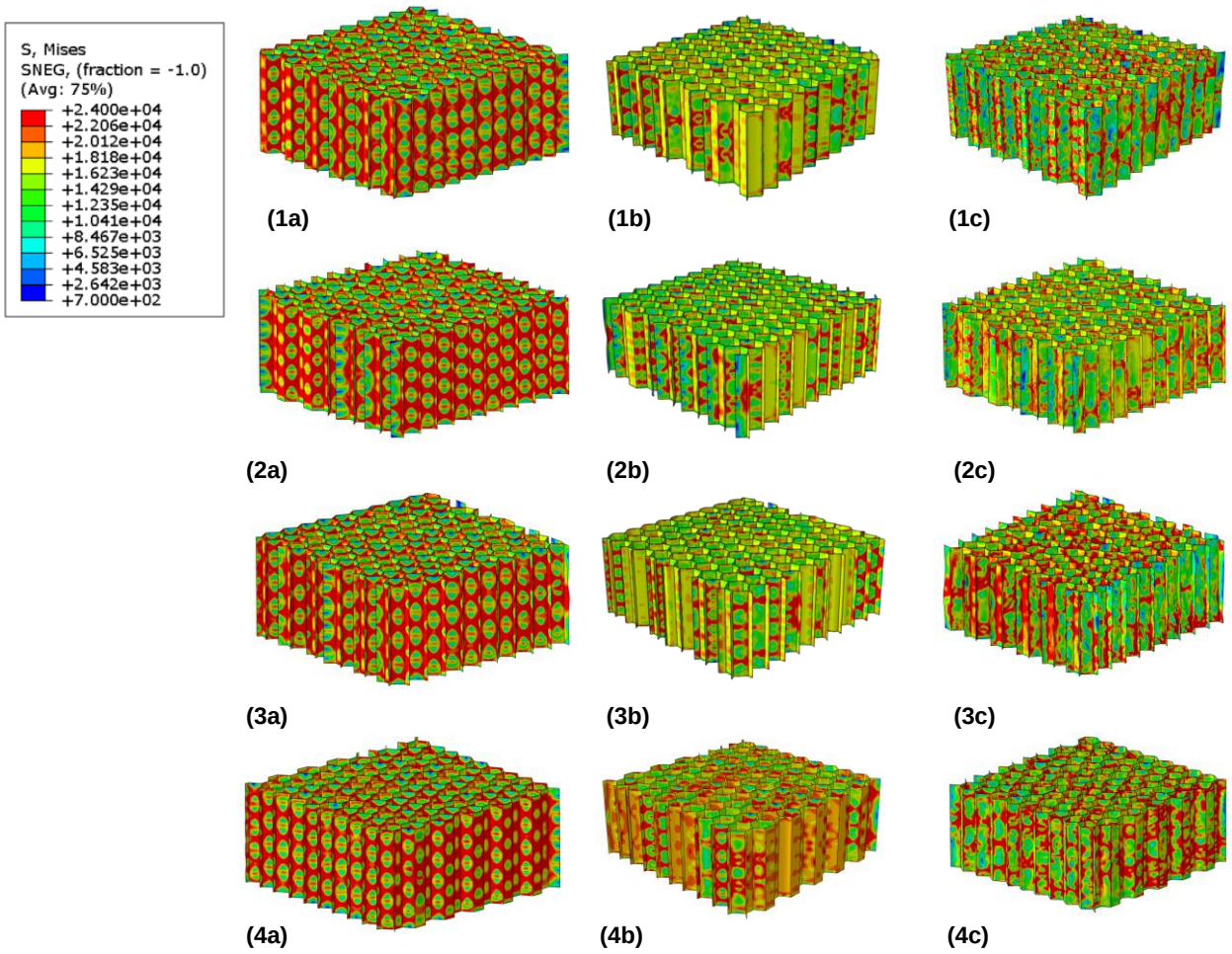

Fig. 18 Contour plots showing von-mises stresses for 10x11 cell models (1) under-expanded 1, (2) under-expanded 2, (3) over-expanded 1, and (4) over-expanded 2 batches with imperfection sources of (a) angle variation (b) in-plane curvature (c) as-manufactured.

V. Conclusions

The decoupling of imperfections measured from X-ray CT indicated that in the full specimen models with in-plane curvature observed to have stabilizing effect on the buckling response whereas imperfections with angle variations the straight cell walls lead to earlier elastic buckling followed by the on-set of yielding in the aluminum foils. The inclusion of through-thickness imperfections (along the Z-direction) resulted in the largest drop in stiffness.

Localization of failure for the finite element model with as-manufactured imperfection cases was dominated by the amplification of initial imperfections prior to collapse of the honeycomb core cells this is clearly observed by the non-linear elastic response prior to the initiation of yielding. The progression of yielding and collapse creates the softening response that is depicted in the pre-peak collapse. The finite element models were within predict compression strength within 5 percent of the experimental tests. The structural stiffness was under predicted in the finite element models, yet the compression behavior trends between batches with unique manufacturing induced imperfections were maintained. For better prediction of the post-peak response a more accurate material model of the 5052 aluminum foil needs to be considered.

VI. Acknowledgments

This work was funded by NASA Fellowship Activity Award (Grant number 80NSSC18K1700). Authors wish to thank ASG Lab at NASA Glenn for assistance with 3D CT imaging and Peter A. Bonacuse, Dr. Cheryl Bowman, and Bill Brown at NASA Glenn Research Center for the assistance with experimental testing. NASA Space Launch System program's support for Dr. Bergan and Dr. Pineda participation in this project is acknowledged. The San Diego ARCS chapter and the SDSU University Graduate Fellowship for current and future funding for this research.

References

[1] Gibson, L. J., "Cellular solids," *Mrs Bulletin*, Vol. 28, No. 4, 2003, pp. 270-274.
[2] Gibson, L. J., et al., "The mechanics of two-dimensional cellular materials," *Proceedings of the Royal Society of London. A. Mathematical and Physical Sciences*, Vol. 382, No. 1782, 1982, pp. 25-42.
[3] Gibson, L. J., and Ashby, M. F., "The mechanics of three-dimensional cellular materials," *Proceedings of the Royal Society of London. A. Mathematical and Physical Sciences*, Vol. 382, No. 1782, 1982, pp. 43-59.
[4] Ashby, M. F., and Medalist, R. F., "The mechanical properties of cellular solids," *Metallurgical Transactions A*, Vol. 14, No. 9, 1983, pp. 1755-1769.
[5] Kuenzi, E. W., "Mechanical properties of aluminum honeycomb cores," 1962.
[6] Triantafyllidis, N., and Schraad, M. W., "Onset of failure in aluminum honeycombs under general in-plane loading," *Journal of the Mechanics and Physics of Solids*, Vol. 46, No. 6, 1998, pp. 1089-1124.
[7] Wang, Z., et al., "On the influence of structural defects for honeycomb structure," *Composites Part B: Engineering*, Vol. 142, 2018, pp. 183-192.
[8] McFarland, R. K. "Hexagonal cell structures under post-buckling axial load," *AIAA journal*, Vol. 1, No. 6, 1963, pp. 1380-1385.
[9] Wierzbicki, T. "Crushing analysis of metal honeycombs," *International Journal of Impact Engineering*, Vol. 1, No. 2, 1983, pp. 157-174.
[10] Wierzbicki, T., and Wlodzimierz, A., "On the crushing mechanics of thin-walled structures," Journal of Applied Mechanics, Vol. 50, No. 4, 1983, pp. 727-734.
[11] Wilbert, A., Jang, W.Y., Kyriakides, S. and Floccari, J. F., "Buckling and progressive crushing of laterally loaded honeycomb," *International Journal of Solids and Structures*, Vol. 48, No. 5, 2011, pp. 803-816.
[12] Jang, W. Y., & Kyriakides, S., "On the buckling and crushing of expanded honeycomb," *International Journal of Mechanical Sciences*, Vol. 91, 2015, pp. 81-90.
[13] Asprone, D., Auricchio, F., Menna, C., Morganti, S., Prota, A. and Reali, A., "Statistical finite element analysis of the buckling behavior of honeycomb structures," *Composite Structures*, Vol. 105, 2013, pp. 240-255.
[14] Campbell, F. C., *Manufacturing Processes for Advanced Composites*, Elsevier, London, pp. 267-277
[15] Tavares, S. S., Michaud, V., and Manson, J.-A. E., "Through Thickness Air Permeability of Prepregs During Cure," *Composites Part A*, Vol. 40, No. 10, 2009, pp. 1587–1596.
[16] Tavares, S. S., Michaud, V., and Manson, J.-A. E., "Assessment of Semi-Impregnated Fabrics in Honeycomb Sandwich Structures," *Composites Part A*, Vol. 41, No. 1, 2010, pp. 8–15.
[17] Grady, L. "Random walks for image segmentation." *IEEE transactions on pattern analysis and machine intelligence*, Vol. 28, No. 11, 2006, pp. 1768-1783.
[18] Rivera, A. X., Venkataraman, S., Hyonny, K., Pineda, E. J. and Bergan, A. "Characterization and Modeling of Cell Wall Imperfections in Aluminum Honeycomb Cores using X-ray CT Imaging". *AIAA Scitech 2021 Forum*, 2021, p. 1620.
[19] Lerch, B. A. "Properties of 5052 Aluminum for Use as Honeycomb Core in Manned Spaceflight." NASA/TM, No. 219753, 2018.
[20] ASTM Standards, "C365-03: Standard test method for Flatwise Compressive Properties of Sandwich cores," *Annual Book of ASTM Standards*, 2018.
[21] Simulia, Abaqus Analysis User's Guide. Version 2022.